# The Pyroptosis Related Genes Signature Predicts Prognosis and Immune Infiltration of Tumor microenvironment in Hepatocellular carcinoma

**Guoxu Fang** ( guoxufang2020@163.com )
Mengchao Hepatobiliary Hospital of Fujian Medical University
**Qinghua Zhang**
The Graduate School of Fujian Medical University
**Jianhui Fan**
Mengchao Hepatobiliary Hospital of Fujian Medical University
**Zongren Ding**
Mengchao Hepatobiliary Hospital of Fujian Medical University
**Jun Fu**
Mengchao Hepatobiliary Hospital of Fujian Medical University
**Yijun Wu**
The Graduate School of Fujian Medical University
**Yongyi Zeng**
Mengchao Hepatobiliary Hospital of Fujian Medical University
**Jingfeng Liu**
Mengchao Hepatobiliary Hospital of Fujian Medical University

**Research Article**

**Keywords:** HCC, Prognosis, Pyroptosis, Overall survival, Immune infiltration

**Posted Date:** May 24th, 2022

**DOI:** https://doi.org/10.21203/rs.3.rs-1644201/v1

**The Pyroptosis Related Genes Signature Predicts Prognosis and Immune Infiltration of Tumor microenvironment in Hepatocellular carcinoma**

Guoxu Fang, ab,1
Qinghua Zhang, c,1
Jianhui Fan, d,1
Zongren Ding, ab,
Jun Fu, ab
Yijun Wu, c
Yongyi Zeng, a,*
Jingfeng Liu, abe, *

a Department of Hepatopancreatobiliary Surgery, Mengchao Hepatobiliary Hospital of Fujian Medical University, Fuzhou 350025, China.
b The Big Data Institute of Southeast Hepatobiliary Health Information, Mengchao Hepatobiliary Hospital of Fujian Medical University, Fuzhou 350025, China,
c The Graduate School of Fujian Medical University, Fuzhou, 350108, China
d Department of Hepatology for Pregnancy, Mengchao Hepatobiliary Hospital of Fujian Medical University, Fuzhou 350025, China.
e Department of Hepatopancreatobiliary Surgery, Fujian Medical University Cancer Hospital, Fujian Cancer Hospital, Fuzhou 350014, China.

1 These authors contributed equally to this work.
* Correspondence author.
Corresponding author:
Yongyi Zeng, MD, PhD, Department of Hepatopancreatobiliary Surgery, Mengchao Hepatobiliary Hospital of Fujian Medical University, Xihong Road 312, Fuzhou 350025, China. Tel (fax): +86 591 8370 5927. E-mail: lamp197311@126.com.
Jingfeng Liu, MD, PhD, Department of Hepatopancreatobiliary Surgery, Mengchao Hepatobiliary Hospital of Fujian Medical University, Xihong Road 312, Fuzhou 350025, China. Tel (fax): +86 591 8370 5927. E-mail: drjingfeng@126.com.

**Abstract**

Hepatocellular carcinoma (HCC) is a particularly heterogeneous tumor. It has a very poor prognosis. Pyroptosis has been demonstrated in recent years to be an inflammatory form of programmed cell death. However, the relationship between the expression of pyroptosis related genes (PRGs) and prognosis of HCC is still unclear. The development of a specific PRGs prognostic model is important if we want to improve therapeutic effect of tumor. In this study, we identified 42 PRGs that were differentially expressed between HCC and peripheral normal tissues and exhibited the mutation frequency, classification, the location of copy number variation (CNV) alteration and the CNV variation frequency of PRGs. Two clusters were distinguished by the consensus clustering analysis based on the 42 differentially expressed genes (DEGs). The result show that there were significant differences in clinical features (including T stage, grade, gender, stage) among different clusters. KM curve analysis show that cluster 1 had a better prognosis than cluster 2. The prognostic

value of PRGs for survival was evaluated to construct a multigene signature using The Cancer Genome Atlas (TCGA) cohort. By applying the univariate analysis and multivariate analysis method, a 10-gene signature was built and all HCC patients in the TCGA cohort were divided into low- risk group and high-risk group. HCC patients in the high-risk group showed significantly lower survival possibilities than those in the low-risk group (P<0.001). Utilizing the median risk score from the TCGA cohort, HCC patients from Gene Expression Omnibus (GEO) cohort (GSE14520) were divided into two risk subgroups. The result showed that overall survival (OS) time was decreased in the high-risk group (P=0.027). Combined with the clinical characteristics, the risk score was found to be an independent factor for predicting the OS of HCC patients. Then, for evaluating the prognostic prediction value of the model, ROC curve and survival analysis were performed. Finally, we constructed a PRGs clinical characteristics nomogram to furtherly predict HCC patient survival probability. There were significant differences in immune cell infiltration, GSEA enrichment pathway, IC50 of chemotherapeutics, PRGs mutation frequency, GO and KEGG analysis between high-risk group and low-risk group. This work suggests PRGs signature plays a crucial role in HCC. The exploration may assist in identifying novel biomarkers and assist HCC patients in predicting their prognosis, clinical diagnosis, and management.

**Keywords:** HCC, Prognosis, Pyroptosis, Overall survival, Immune infiltration

**Abbreviations**

HCC: Hepatocellular carcinoma, TCGA: the cancer genome atlas, GEO: gene expression omnibus, FPKM: fragments per kilobase million, DEG: differential expression gene, FDR: false discovery rate, RS: Risk score, OS: overall survival, ROC: receiver operating characteristic, KM: kaplan–meier, GSEA: gene set enrichment analysis, GO: gene ontology, KEGG: kyoto encyclopedia of genes and genomes, HR: hazard ration, 95% CI: 95% confidence interval, AUC: area under the curve.

## Introduction

Hepatocellular carcinoma (HCC) is one of the most common gastrointestinal malignancies worldwide and has a high incidence and mortality. According to the latest data from the International Cancer Research Agency, there are approximately 841,080 new cases and 781,631 deaths every year, and HCC ranks seventh and third among all malignant tumors in morbidity and mortality, respectively[1]. HCC has severe malignant course, various symptoms, difficult treatment and poor prognosis. HCC is a serious threat to human health and economic development. However, there is a lack of effective drugs and special treatments for HCC. With the progress of precision medicine and modern molecular biotechnology, pyroptosis has been gradually revealed by researchers, and it has been successively found that pyroptosis plays an important role in the progress of HCC and other tumor diseases[2]. Pyroptosis is a programmed cell death, and inflammasome and caspase play an important role in the process of pyroptosis[3]. Pyroptosis pathways include canonical pyroptotic pathways mediated by caspase-1 dependence and non-canonical pyroptotic pathways mediated by caspase-4, -5, and -11. Caspase-1 or Caspase-4, -5, and -11 cleave gasdermin family protein D (GSDMD). The N-terminal and C-terminal structural domains of GSDMD are separated, and the released N-terminal fragments recognize and bind phospholipids molecules on the cell membrane, forming membrane pores in the cell membrane, causing cell osmotic pressure change, cell swelling and cell membrane lysis, resulting in osmotic dissolution of cells, namely,

pyroptosis[4]. The function of pyroptosis is different in different stages of HCC development. With the increasing incidence of liver diseases, it has recently become a serious health issue. Some liver diseases is gradually converted to cirrhosis, as well as liver cancer, which can become a massive threat to human health worldwide[5]. Recent studies have reported that pyroptosis can play significant roles in the progression of liver diseases[2]. Infectious hepatic diseases - liver fibrosis - HCC is the progression of liver disease with three stages, infectious hepatic diseases and liver fibrosis are the initial factors of HCC and liver fibrosis belongs to the pre-cancerous phase of HCC. It is important to control and prevent the progression of infectious hepatic diseases and liver fibrosis to HCC. Hepatocyte death and inflammatory response are the main causes of liver fibrosis[6]. Wree demonstrated that pyroptosis induced by NLRP3 was able to increase the expression of CTGF, TIMP1 and enhance collagen deposition. It was reported that NLRP3- initiated pyroptosis resulted in more severe liver inflammation and fibrosis. In contrast, the NLRP3 deficiency can protect liver from thioacetamide (TAA) or carbon tetrachloride---induced liver fibrosis[7]. A growing number of studies suggest that pyroptosis also plays an important role in the development of tumours. It has been reported that inflammatory vesicles, gasdermin proteins, and proinflammatory cytokines, which are key components of pyroptosis, are associated with tumourigenesis, invasion, and metastasis[8]. In the precancerous phase of HCC, the accumulation of inflammatory corpuscles and inflammatory factors will aggravate the transition of cirrhosis to HCC. However, when liver disease enters tumor stage, pyroptosis is inhibited, forming an internal malignant tumor microenvironment, blocking the cancer cell death and accelerating the deterioration of HCC. Analysis of relevant clinical trial data showed that NLRP3 inflammasome components were either completely lost or significantly down-regulated in HCC, and its deficiency was associated with advanced cancer and poor differentiation, suggesting that down-regulated NLRP3 inflammasome expression was involved in malignant progression of HCC[4]. Some recent studies that highlight a previously unappreciated role of gasdermin-mediated pyroptosis to promote anti-tumor immunity and identifies gasdermin E as a tumor suppressor. Immune elimination of tumor cells by natural killer cells and cytotoxic T lymphocytes, which is the final key event in anti-tumor immunity[9]. Pyroptosis is closely related to cancer. An in-depth study on the mechanism of pyroptosis and its relationship with cancer is helpful to understand the pathogenesis and development of cancer and can provide a new method for cancer prevention and treatment[10-12]. Given the existing findings, we know that pyroptosis plays an important role in the development of tumours and antitumour processes. However, its specific functions in HCC have been less studied. Thus, we performed a systematic study to explore the prognostic value of these genes, and study the correlations between pyroptosis and the tumour immunotherapy.

## Materials and methods

### Datasets

The TCGA-liver cancer dataset consisted of the RNA-seq data, somatic mutation data, and copy number variation (CNV) of 374 liver cancer tissue and 50 adjacent normal samples and related clinical characteristics were downloaded from the TCGA database. GSE14520 contained the gene expression data with clinical characteristics was downloaded from the GEO database. The TCGA dataset was enrolled as a training cohort and the GEO dataset was regarded as the external validation cohort. As these data were open-access, therefore, the ethical approval by an ethics committee was not required.

**Identification of differentially expressed PRGs**

We extracted 52 PRGs from prior reviews [13-16], previous pyroptosis-related studies[17-30] and MSigDB database v7.4[31] (listed in Supplementary Table S1). The TCGA-liver cancer dataset consisted of the RNA-seq data of 374 liver cancer tissue and 50 adjacent normal samples was used to identify the DEGs between normal and tumour tissues. The expression data in both datasets were normalized to fragment per kilobase million (FPKM) values before comparison. The "limma" package was used to identify DEGs with P value <0.05. The DEGs are notated as follows: * if P < 0.05, ** if P < 0.01, and *** if P < 0.001. A PPI network for the DEGs was constructed with Search Tool for the Retrieval of Interacting Genes (STRING), version 11.0.

**Unsupervised Clustering based on PRGs**

Based on the expression of PRGs, unsupervised cluster analysis was performed to identify different pyroptosis type, and patients were divided into different groups for subsequent analysis. The ConsenSuClusterPlus R package was used to process the above analysis, and 2,000 repeats were performed to ensure the stability of the classification. The correlation between different clusters and clinical information was further determined by Chi-square test. The overall survival (OS) of each cluster was performed using the Kaplan–Meier (KM) survival curve.

**Development and validation of the PRGs prognostic model**

To assess the prognostic value of the PRGs, we further employed Cox regression analysis to evaluate the correlations between each gene and survival status in the TCGA cohort. Univariate and multivariate COX analyses were performed on the PRGs. Ultimately, the ten genes associated with prognosis and pyroptosis and their coefficients were identified. The expression data of the PRGs associated with prognosis in the training cohorts (TGCA dataset) were used in constructing a risk score model. External validation cohorts (GSE14520) were then used to verify the reliability of the risk score model. The risk score was calculated after centralization and standardization of the TCGA expression data, and the risk score formula was as follows: Risk Score= $\sum_{i}^{10} Xi \times Yi$ (X: coefficients, Y: gene expression level). The TCGA HCC patients were divided into low-risk group and high-risk group according to the median risk score. A log-rank test was used in comparing the survival difference between the two groups. The overall survival (OS) of each group was performed using the Kaplan–Meier (KM) survival curve. The "survival", "survminer" and "timeROC" R packages were employed to perform 1,3,5-year ROC curve analysis.

**Independent prognostic analysis of the risk score**

We extracted the clinical information (age, gender, grade, stage, T stage, N stage, M stage) of patients in the TCGA cohort. These variables were analyzed in combination with the risk score in our regression model. Univariate and multivariable Cox regression models were employed for the analysis.

**Correlation Analysis between Immunity and the Risk Groups**

The lollipop of immune responses is based on XCELL, TIMER, QUANTISEQ, MCPCOUNTER, EPIC, CIBERSORT, and CIBERSORT-ABS algorithms to analyze the Spearman correlation between risk score values and tumor-infiltrating immune cells (TIIC). In addition, the heatmap depicts the component differences of immune cells between the high- and low-risk groups, as well

as risk score values.

**Function Analysis Between High- and Low-Risk Groups**

GSEA was used to investigate the biological function of PRGs. To assess the signature in clinical trials for HCC treatment, we utilized R ggplot2 and pRRophetic packages to calculate the lower half inhibitory concentration (IC50) of commonly used chemotherapeutic drugs (such as lapatinib) in TCGA-HCC. Moreover, somatic mutations were explored among high- and low-risk groups using maftools, an R package for analyzing and visualizing mutation annotation format (MAF) files from large-scale sequencing studies.

**Functional enrichment analysis of the DEGs between the low-risk group and high-risk group**

HCC patients in the TCGA cohort were stratified into two subgroups according to the median risk score. The DEGs between the low- risk group and high-risk group were filtered according to specific criteria ($|\log2FC| \geq 1$ and FDR $< 0.05$). Based on these DEGs, GO and KEGG analyses were performed by applying the "clusterProfiler" package. The "gsva" package was utilized to conduct the ssGSEA to calculate the scores of infiltrating immune cells and to evaluate the activity of immune-related pathways.

**Quantitative Reverse Transcription Polymerase Chain Reaction**

Cell total RNA was extracted using Trizol reagent (Invitrogen, USA) following the manufacturer's instructions. The quantity and quality of extracted RNA were assessed by the spectrophotometric (Dojindo Laboratories, Kumamoto, Japan) determination of absorbance ratio (A260/A280). Then, the prepared RNA was reversely transcribed into cDNA using reverse transcriptase (Invitrogen, USA) and random primers. One microliter of synthesized cDNA was used in each qPCR reaction. SYBR Green-based qRT-PCR was subsequently executed on ABI PRISM 7300HT Sequence Detection System (Applied Biosystems, USA). β-Actin was used as a control for normalization. Primers used in RT-PCR were listed in Supplementary Table S2.

**Statistical Analysis**

R software (version 4.0.2) was used to complete all the statistic work. OS was calculated by the KM method, and the differences between the groups were compared by using the log-rank test. Cox proportional hazard model was used to analyze the significant PRGs affecting OS. $P < 0.05$ was considered statistically significant.

**Results**

**Differentially Expressed PRGs in the TCGA Cohort and Landscape of genetic and expression variation of PRGs in HCC.**

The workflow flow chart of data analysis is shown in Fig. 1. The 52 PRGs expression levels were compared in TCGA data from 50 normal and 374 tumor tissues, and we identified 42 differentially expressed genes (DEGs). Among them, 5 genes (IL1B, AIM2, IL6, NLRP3, NLRP6) were downregulated while 37 other genes (BAK1, BAX, CASP3, CASP4, CHMP2A, CHMP2B, CHMP3, CHMP4A, CHMP4B, CHMP4C, CHMP6, CHMP7, CYCS, GSDMD, GSDME, HMGB1, IL1A, IRF2, TP53, TP63, CASP6, CASP8, CASP9, GPX4, GSDMA, GSDMB, GSDMC, NLRP1, NLRP7, NOD1, NOD2, PJVK, PLCG1, PRKACA, PYCARD, SCAF11, TIRAP) were enriched in the tumor

group. The RNA levels of these genes are presented in Fig. 2A. We then demonstrated the incidence of copy number variations and somatic mutations of 52 PRGs in HCC. As shown in Fig. 2B, 157 of 364 (43.13%) HCC samples demonstrated genetic mutations. Missense mutation was the most common variant classification (Fig. 2B). The results also demonstrated TP53 as the gene with the highest mutation frequency, followed by NLRP2 and NLRP3, among the 52 PRGs (Fig. 2B). Fig. 2C presents the location of CNV alterations of these 52 PRGs on chromosomes. We also investigated CNV alteration frequency, which revealed that these 52 PRGs showed prevalent CNV alterations. More than half of the 52 PRGs had copy number amplification, while the CNV deletion frequencies of CASP9, CASP3, HMGB1, ELANE, CASP6, IRF2, GSDMB, GSDMA, GPX4, CASP4, CASP5, CASP1, IL18, TIRAP, CHMP2B, NLRP1, TP53 and CHMP7 were widespread (Fig. 2D).

To further explore the interactions of these PRGs, we conducted a protein–protein interaction (PPI) analysis, and the results are shown in Fig. S1A. The minimum required interaction score for the PPI analysis was set at 0.9 (the highest confidence) and we determined that IL1B, NLRP3, PYCARD, CASP8, CASP3, TP53, CHMP2A were hub genes. The correlation network containing all PRGs is presented in Fig. S1B (red: positive correlations; blue: negative correlations).

**Tumour classification based on the DEGs**

To explore the connections between the expression of the 42 pyroptosis-related DEGs and HCC clusters, we performed a consensus clustering analysis with 374 HCC patients in the TCGA cohort. By increasing the clustering variable (k) from 2 to 10, we found that when k=2, the intragroup correlations were the highest and the intergroup correlations were low, indicating that the 374 HCC patients could be well divided into two clusters based on the 42 DEGs (Fig. 3A). The gene expression profile and the clinical features are presented in a heatmap, and we found that the distributions of T stage, stage, grade and gender in the two cluster groups were different, while the distributions of N stage, M stage and age were not significantly different (Fig. 3B). There is a significant difference in the overall survival (OS) time of two clusters ($P<0.001$, Fig. 3C).

**Development of a prognostic gene model in the TCGA cohort**

A total of 374 HCC samples were matched with the corresponding patients who had complete survival information. Univariate Cox regression analysis was used for screening of the survival-related pyroptosis genes (Fig. 4A). Then, these genes were performed by multivariate Cox regression analysis. The 10 genes (BAK1, BAX, CHMP2A, GSDME, IL1A, TP53, TP63, GPX4, PRKACA and SCAF11) were identified and used in subsequent modeling. The risk score was calculated as follows: risk score = (0.368611051021708 * expression of BAK1) + (0.308688517099686 * expression of BAX) + (-0.52007432297355 *expression of CHMP2A) + (0.330587747807719 * expression of GSDME) + (-0.807361948750797 * expression of IL1A) + (-0.323671479794998 * expression of TP53) + (-0.604855494168515* expression of TP63) + (0.512445054990862 * expression of GPX4) + (-0.283264209118667 * expression of PRKACA) + (0.432681763927682 * expression of SCAF11). Based on the median score calculated by the risk score formula, 374 patients were equally divided into low-risk group and high-risk group (Fig. 4B). Patients in the high-risk group had more deaths and a shorter survival time than those in the low-risk group (Fig. 4C). A notable difference in OS time was detected between the low-risk group and high-risk group ($P < 0.001$, Fig. 4D). Time dependent receiver operating characteristic (ROC)

analysis was applied to evaluate the sensitivity and specificity of the prognostic model, and we found that the area under the ROC curve (AUC) was 0.766 for 1-year, 0.694 for 3-year, and 0.676 for 5-year survival (Fig. 4E).

**External validation of the risk signature**

A total of 221 HCC patients from a Gene Expression Omnibus (GEO) cohort (GSE14520) were utilized as the validation set. Based on the median risk score in the TCGA cohort, 108 patients in the GEO cohort were classified into the low-risk group, while the other 113 patients were classified into the high-risk group (Fig. 5A). Patients in the low-risk group were found to have longer survival time and lower death rate than those in the high-risk group (Fig. 5B). In addition, Kaplan–Meier analysis also indicated a significant difference in the survival rate between the low-risk group and high-risk group (P= 0.027, Fig. 5C). ROC curve analysis of the GEO cohort showed that our model had good predictive efficacy (AUC= 0.557 for 1-year, 0.571 for 3-year, and 0.637 for 5-year survival) (Fig. 5D).

**Independent prognostic value of the risk model**

We used univariate and multivariable Cox regression analyses to evaluate whether the risk score derived from the gene signature model could serve as an independent prognostic factor. The univariate Cox regression analysis indicated that the risk score was an independent factor predicting poor survival in the TCGA cohort (HR= 1.601, 95% CI: 1.374–1.864, Fig. 6A). The multivariate analysis also implied that, after adjusting for other confounding factors, the risk score was an independent prognostic factor for patients with HCC in the TCGA cohort (HR= 1.485, 95% CI: 1.261–1.750, Fig. 6B). In addition, we generated a heatmap of clinical features for the TCGA cohort and found that the T stage and grade were differently distributed between the low-risk group and high-risk group (Fig. 6C).

**Establishment and evaluation of a nomogram for predicting patient 1-year, 3-year and 5-year OS**

Four prognostic factors were combined to establish a nomogram for predicting 1-year, 3-year and 5-year OS based on the TCGA dataset (Fig. 7A). The calibration curves for predicting 1-year, 3-year and 5-year OS were in good agreement with the observed values (Fig. 7B). The areas under the ROC curves for predicting 1-year, 3-year and 5-year OS were 0.81, 0.80 and 0.76, respectively (Fig. 7C).

**The relationship between prognostic signature and immune response**

Firstly, we examined component differences of immune cells between high- and low-risk groups, as well as risk score values. A detailed Spearman correlation analysis was performed using different algorithms, with a resulting lollipop shape, as displayed in Fig. 8A. The results indicate that most immune cells are positively correlated with the risk score, consistent with our GSEA finding that the high-risk group is predominantly enriched in immune-related pathways. The heatmap demonstrated that the infiltration of most immune cells was higher in the high-risk group than in the low-risk group (Fig. 8B). We further elucidated the correlation of PRGs expression with each type of immune cell infiltration (Fig. S2).

**Gene set enrichment analysis (GSEA) and lower half inhibitory centration (IC50) of chemotherapeutic drugs between the high- and low-risk group**

Gene set enrichment analysis (GSEA) has an advantage in exploring the involved signaling pathways. GSEA revealed that the genes in the high-risk group of TCGA cohorts were significantly enriched in tumor and immune-related pathways such as B cell receptor signaling pathway, T cell receptor signaling pathway, P53 signaling pathway, Pathways in cancer, Cell cycle. In contrast, the low-risk group genes were significantly enriched in metabolism-related pathways such as Complement and coagulation cascades, Drug metabolism cytochrome p450, Retinol metabolism, Fatty acid metabolism, Linoleic acid metabolism (Fig. 9A). Therefore, we speculate that our prognostic signature is related to tumor immunity and metabolism. Following that, we examined whether the risk score can predict the sensitivity of patients to chemotherapy and found that a low-risk score was linked to an IC50 of chemotherapeutics such as Gemcitabine, Nilotinib, Camptothecin, Tipifarnib ($p < 0.001$), whereas a high-risk score was linked to Axitinib, Dasatinib, Erlotinib, Lapatinib ($p < 0.001$), implying that PRGs signature served as a prospective predictor for chemosensitivity (Fig. 9B).

**Functional analyses based on the risk model**

To further explore the differences in the gene functions and pathways between the subgroups categorized by the risk model, we utilized the “limma” R package to extract the DEGs by applying the criteria FDR < 0.05 and $|\log2FC| \geq 1$. In total, 35 DEGs between the low-risk group and high-risk group in the TCGA cohort were identified. Gene ontology (GO) enrichment analysis and Kyoto Encyclopaedia of Genes and Genomes (KEGG) pathway analysis were then performed based on these DEGs. The results indicated that the DEGs were mainly correlated with the drug metabolic process (Fig. 10A and B). Furthermore, different risk groups should be treated with different medications. Meanwhile, the top 2 driver genes TP53 and CTNNB1 were significantly different between high (Fig. S3A) and low-risk groups (Fig. S3B).

**Validated PRGs between HCC Tissues and Adjacent Normal Tissues**

To explore the expression of BAK1, BAX, CHMP2A, GSDME, IL1A, TP53, TP63, GPX4, PRKACA and SCAF11 in HCC tissues, we detected PRGs expression in 30 patients' tissues by PCR assay. The results of qRT-PCR suggested that BAK1, BAX, CHMP2A, GSDME, IL1A, TP53, TP63, GPX4, PRKACA and SCAF11 are highly expressed in HCC tissues (Fig. 11A-J).

**Discussion**

Pyroptosis, a novel form of programmed cell death, was found to play a dual-role in different stages of HCC development and therapeutic mechanisms in recent years. Studies have shown that NLRP3 inflammasome activation results in hepatocyte pyroptosis, liver inflammation and fibrosis[7]. Other study demonstrated that the expression of all of the NLRP3 inflammasome components was either completely lost or significantly downregulated in HCC. The deficiency of NLRP3 was correlated closely with advanced stages and poor pathological differentiation. In other words, loss of NLRP3 inflammasome leads to a decrease in pyroptosis, which further promotes the progression of HCC cells. In conclusion, pyroptosis can promote and inhibit tumor genesis. NLRP3 inflammasome mediated pyroptosis may inhibit the proliferation and metastasis of HCC, which may be a novel therapeutic strategy[32].

In this study, we first studied the mRNA levels of 52 currently known PRGs in HCC and normal tissues and found that 42 PRGs were differentially expressed. Then, two clusters were produced by the consensus clustering analysis based on the DEGs. The result show that there were significant differences in clinical features (including T stage, grade, gender, stage) among different clusters. KM curve analysis showed that cluster 1 had a better prognosis than cluster 2.

In HCC, the relation of PRGs and the survival time of patients remain unknown. We established a prognostic model based on 10 PRGs (BAK1, BAX, CHMP2A, GSDME, IL1A, TP53, TP63, GPX4, PRKACA and SCAF11) and found that it could predict OS in HCC patients. Lei Hu suggested that chemotherapy-induced pyroptosis was mediated by the BAK/BAX-caspase-3-GSDME pathway, but also showed either BAK or BAX alone can mediate this process. More importantly, they found that GSDME was palmitoylated during chemotherapy-induced pyroptosis[33]. Junhui Yu found that in colon cancer cells, GSDME mediates lobaplatin-induced pyroptosis downstream of the ROS/JNK/Bax-mitochondrial apoptotic pathway and caspase-3/-9 activation[34]. Xiaowei Zhang demonstrated that miltirone inhibited HCC cells growth through BCL2-associated X (BAX)–caspase–GSDME-dependent pyroptotic by regulating ROS/ mitogen-activated and extracellular signal-regulated kinase (MEK)/extracellular regulated protein kinases 1/2 (ERK1/2) pathway[35]. Tatsuya Hattori provided evidence here that CHMP2A depletion induces inducing signaling complexes (iDISC)-mediated noncanonical Caspase-8 activation on immature autophagosomal membranes and inhibits tumor growth in a mouse xenograft model[36]. GSDME was identified as a pore forming molecule, which is activated following caspase-3-mediated cleavage resulting in so-called secondary necrosis following apoptotic cell death, or in primary necrotic cell death without an apoptotic phase, so-called pyroptosis-like[37]. Mingxia Jiang found that the caspase-3/GSDME signal pathway was a switch between apoptosis and pyroptosis in cancer[38]. Junhui Yu suggested that cleavage of GSDME by caspase-3 determines lobaplatin-induced pyroptosis in colon cancer cells[34]. Xiaowei Zhang demonstrated that miltirone induces cell death in hepatocellular carcinoma cell through GSDME dependent pyroptosis[35]. Julia Lachner indicated that expression levels of pro-inflammatory IL1A and IL1B and of the pyroptotic pore-forming gasdermin (GSDM) D were downregulated during terminal differentiation of human keratinocytes in vitro. They screened pyroptosis-related protein families for members with predominant expression in the skin and provide evidence for normal keratinocyte differentiation-associated expression of specific IL1F cytokines and proteins related to pyroptosis[39]. Tianze Zhang found that transcription factor p53 suppresses tumor growth by prompting pyroptosis in non-small-cell lung cancer[40]. N-terminal isoforms of p63 are TAp63 and ΔNp63[41]. The findings of the present study suggested that lncRNA RP1-85F18.6 may trigger colorectal cancer cell proliferation, invasion and cell cycle disruption, and suppress apoptosis and pyroptosis of colorectal cancer cells through regulating ΔNp63 expression[42]. Hong Zhu discussed the recent research findings regarding a protective role for glutathione peroxidase-4 (GPx4) in bacterial infection and polymicrobial sepsis via modulating ferroptosis and pyroptosis, two novel modes of regulated cell death. It is suggested that GPx4, being a requisite gateway to both ferroptosis and pyroptosis, may serve as a critical molecular target for developing effective drugs for controlling infection and sepsis[43]. PRKACA was identified to be PRG and used to construct prognostic risk prediction models in colon adenocarcinoma and glioma [19, 44]. SCAF11 was identified to be PRG and used to construct prognostic risk prediction models in breast cancer[27].

To further assess the prognostic value of these PRGs, prognostic model constructed by 10 PRGs

in the TCGA database was validated to perform well in an external dataset (GSE14520). We revealed that the relationship between PRGs signature and immune response by TIMER, CIBERSORT, CIBERSORT-ABS, QUANTISEQ, MCPCOUNTER, XCELL and EPIC algorithms[45]. GSEA revealed that the genes in the high-risk group of TCGA cohorts were significantly enriched in tumor and immune-related pathways. In contrast, the low-risk group genes were significantly enriched in metabolism-related pathways. Therefore, we speculate that our prognostic signature is related to tumor immunity and metabolism. Following that, we examined whether the risk score can predict the sensitivity of patients to chemotherapy and found that a low-risk score was linked to IC50 of chemotherapeutics such as Gemcitabine, Nilotinib, Camptothecin, Tipifarnib ($p < 0.001$), whereas a high-risk score was linked to Axitinib, Dasatinib, Erlotinib, Lapatinib ($p < 0.001$), implying that signature served as a prospective predictor for chemosensitivity. The functional analyses indicated that the DEGs between the low-risk group and high-risk group were related to drug metabolic process. The results suggest that patients in different risk groups may need to be treated differently. Furthermore, we detected PRGs expression in 30 patients' tissues by PCR assay. The results of qRT-PCR suggested that BAK1, BAX, CHMP2A, GSDME, IL1A, TP53, TP63, GPX4, PRKACA and SCAF11 are highly expressed in HCC tissues.

There is little current research on pyroptosis, especially on its mechanism in HCC. Tumors were divided into two clusters based on PRGs. Different clusters show significant differences in survival probability and clinical characteristics (including T stage, grade, gender, stage). The prognosis of two clusters is also different. Then, we confirmed the prognostic value of PRGs and provided theoretical support for future research. In summary, our study demonstrated that pyroptosis is closely connected to HCC because most of the pyroptosis related genes between normal and HCC tissues were differently expressed. Moreover, the score generated from our risk signature based on 10 PRGs was an independent risk factor for predicting OS. The low-risk group and high-risk group show significant differences in the immune cell infiltration and activated pathways. Our study provides a novel gene signature for predicting the prognosis of HCC patients and offers a significant basis for future studies of the relationships between PRGs and immunity in HCC.

## Declarations

### Ethics approval and consent to participate

The experimental protocol was established, according to the ethical guidelines of the Helsinki Declaration and was approved by the Ethics Committee of Mengchao Hepatobiliary Hospital of Fujian Medical University. Written informed consent was obtained from individual or guardian participants.

### Consent for publication

Not applicable.

### Availability of data and materials

All data included in this study are available upon request by contact with the corresponding author.

### Competing interests

The authors declare no competing interests.

### Funding

This research project is supported by natural Science Foundation of Fujian Province (2021J011283), Fujian Provincial Clinical Research Center for Hepatobiliary and Pancreatic Tumors (2020Y2013) and Key Clinical Specialty Discipline Construction Program of Fuzhou (201912002).

**Authors' contributions**

Study concept and design: Guoxu Fang; Qinghua Zhang; jianhui Fan; Yongyi Zeng; Jingfeng Liu

Acquisition, analysis, or interpretation of data: All authors.

Statistical analysis: Guoxu Fang, Qinghua Zhang; jianhui Fan.

Establishment of the model: Guoxu Fang, Qinghua Zhang; jianhui Fan.

Drafting of the manuscript: Guoxu Fang, Qinghua Zhang; jianhui Fan.

**Acknowledgements**

The authors acknowledge the members of the department of Department of Hepatopancreatobiliary Surgery, Mengchao Hepatobiliary Hospital of Fujian Medical University, especially Zongren Ding, Jun Fu and Yijun Wu for excellent technical assistance. We are very grateful for data provided by databases such as TCGA, GEO.

**Reference**

[1] F. Bray, J. Ferlay, I. Soerjomataram, R.L. Siegel, L.A. Torre, A. Jemal, Global cancer statistics 2018: GLOBOCAN estimates of incidence and mortality worldwide for 36 cancers in 185 countries, CA Cancer J Clin, 68 (2018) 394-424.

[2] Y.J. Qun Chu , Wei Zhang , Chaoqian Xu , Weijie Du , Gulnara Tuguzbaeva , Ying Qin , Anqi Li , Liangshuan Zhang , Guiyuan Sun , Yongqiao Cai , Qiang Feng , Guiyang Li , Yanyao Li , Zhimin Du , Yunlong Bai , Baofeng Yang, Pyroptosis is involved in the pathogenesis of human hepatocellular carcinoma, Oncotarget, 7 (2016) 84658-84665.

[3] T. Bergsbaken, S.L. Fink, B.T. Cookson, Pyroptosis: host cell death and inflammation, Nat Rev Microbiol, 7 (2009) 99-109.

[4] A. Al Mamun, Y. Wu, C. Jia, F. Munir, K.J. Sathy, T. Sarker, I. Monalisa, K. Zhou, J. Xiao, Role of pyroptosis in liver diseases, Int Immunopharmacol, 84 (2020) 106489.

[5] Y.M. Yang, S.Y. Kim, E. Seki, Inflammation and Liver Cancer: Molecular Mechanisms and Therapeutic Targets, Semin Liver Dis, 39 (2019) 26-42.

[6] H. Guo, M. Xie, C. Zhou, M. Zheng, The relevance of pyroptosis in the pathogenesis of liver diseases, Life Sci, 223 (2019) 69-73.

[7] A. Wree, A. Eguchi, M.D. McGeough, C.A. Pena, C.D. Johnson, A. Canbay, H.M. Hoffman, A.E. Feldstein, NLRP3 inflammasome activation results in hepatocyte pyroptosis, liver inflammation, and fibrosis in mice, Hepatology, 59 (2014) 898-910.

[8] R. Kolb, G.H. Liu, A.M. Janowski, F.S. Sutterwala, W. Zhang, Inflammasomes in cancer: a double-edged sword, Protein Cell, 5 (2014) 12-20.

[9] Z. Zhang, Y. Zhang, J. Lieberman, Lighting a Fire: Can We Harness Pyroptosis to Ignite Antitumor Immunity?, Cancer Immunol Res, 9 (2021) 2-7.

[10] Y. Tan, Q. Chen, X. Li, Z. Zeng, W. Xiong, G. Li, X. Li, J. Yang, B. Xiang, M. Yi, Pyroptosis: a new paradigm of cell death for fighting against cancer, J Exp Clin Cancer Res, 40 (2021) 153.

[11] L. Wang, X. Qin, J. Liang, P. Ge, Induction of Pyroptosis: A Promising Strategy for Cancer Treatment, Front Oncol, 11 (2021) 635774.

[12] D. Wu, S. Wang, G. Yu, X. Chen, Cell Death Mediated by the Pyroptosis Pathway with the Aid of Nanotechnology: Prospects for Cancer Therapy, Angew Chem Int Ed Engl, 60 (2021) 8018-8034.

[13] T.-D.K. Si Ming Man Regulation of inflammasome activation, Immunol Rev, 265 (2015) 6-21.

[14] B. Wang, Q. Yin, AIM2 inflammasome activation and regulation: A structural perspective, J Struct Biol, 200 (2017) 279-282.

[15] R. Karki, T.D. Kanneganti, Diverging inflammasome signals in tumorigenesis and potential targeting, Nat Rev Cancer, 19 (2019) 197-214.
[16] X. Xia, X. Wang, Z. Cheng, W. Qin, L. Lei, J. Jiang, J. Hu, The role of pyroptosis in cancer: pro-cancer or pro-"host"?, Cell Death Dis, 10 (2019) 650.
[17] Y. Cao, J. Xie, L. Chen, Y. Hu, L. Zhai, J. Yuan, L. Suo, Y. Shen, R. Ye, J. Li, Z. Gong, Y. Dong, W. Bao, H. Li, M. Wang, Construction and Validation of a Novel Pyroptosis-Related Gene Signature to Predict the Prognosis of Uveal Melanoma, Front Cell Dev Biol, 9 (2021) 761350.
[18] W. Lin, Y. Chen, B. Wu, Y. Chen, Z. Li, Identification of the pyroptosisrelated prognostic gene signature and the associated regulation axis in lung adenocarcinoma, Cell Death Discov, 7 (2021) 161.
[19] B. Luo, J. Lin, W. Cai, M. Wang, Identification of the Pyroptosis-Related Gene Signature and Risk Score Model for Colon Adenocarcinoma, Front Genet, 12 (2021) 771847.
[20] L. Qi, R. Xu, L. Wan, X. Ren, W. Zhang, K. Zhang, C. Tu, Z. Li, Identification and Validation of a Novel Pyroptosis-Related Gene Signature for Prognosis Prediction in Soft Tissue Sarcoma, Front Genet, 12 (2021) 773373.
[21] X. Qian, J. Tang, Y. Chu, Z. Chen, L. Chen, C. Shen, L. Li, A Novel Pyroptosis-Related Gene Signature for Prognostic Prediction of Head and Neck Squamous Cell Carcinoma, Int J Gen Med, 14 (2021) 7669-7679.
[22] J. Rao, W. Li, C. Chen, Pyroptosis-Mediated Molecular Subtypes and Tumor Microenvironment Infiltration Characterization in Colon Cancer, Front Cell Dev Biol, 9 (2021) 766503.
[23] W. Wang, S.W. Xu, Y. Teng, M. Zhu, Q.Y. Guo, Y.W. Wang, X.L. Mao, S.W. Li, W.D. Luo, The Dark Side of Pyroptosis of Diffuse Large B-Cell Lymphoma in B-Cell Non-Hodgkin Lymphoma: Mediating the Specific Inflammatory Microenvironment, Front Cell Dev Biol, 9 (2021) 779123.
[24] D. Wei, X. Lan, Z. Huang, Q. Tang, Z. Wang, Y. Ma, L. Wei, Q. Wei, J. Zhao, J. Shen, S. He, J. Song, L. Meng, Q. Tang, Pyroptosis-Related Gene Signature Is a Novel Prognostic Biomarker for Sarcoma Patients, Dis Markers, 2021 (2021) 9919842.
[25] R. Wei, S. Li, G. Yu, X. Guan, H. Liu, J. Quan, Z. Jiang, X. Wang, Deciphering the Pyroptosis-Related Prognostic Signature and Immune Cell Infiltration Characteristics of Colon Cancer, Front Genet, 12 (2021) 755384.
[26] P. Wu, J. Shi, W. Sun, H. Zhang, Identification and validation of a pyroptosis-related prognostic signature for thyroid cancer, Cancer Cell Int, 21 (2021) 523.
[27] D. Xu, Z. Ji, L. Qiang, Molecular Characteristics, Clinical Implication, and Cancer Immunity Interactions of Pyroptosis-Related Genes in Breast Cancer, Front Med (Lausanne), 8 (2021) 702638.
[28] R. Zeng, S. Huang, X. Qiu, Z. Zhuo, H. Wu, L. Jiang, W. Sha, H. Chen, Predicting the Prognosis of Esophageal Adenocarcinoma by a Pyroptosis-Related Gene Signature, Front Pharmacol, 12 (2021) 767187.
[29] M. Zhang, Y. Cheng, Z. Xue, Q. Sun, J. Zhang, A novel pyroptosis-related gene signature predicts the prognosis of glioma through immune infiltration, BMC Cancer, 21 (2021) 1311.
[30] Z. Zhuang, H. Cai, H. Lin, B. Guan, Y. Wu, Y. Zhang, X. Liu, J. Zhuang, G. Guan, Development and Validation of a Robust Pyroptosis-Related Signature for Predicting Prognosis and Immune Status in Patients with Colon Cancer, J Oncol, 2021 (2021) 5818512.
[31] P.T. Aravind Subramanian, Vamsi K Mootha, Sayan Mukherjee, Benjamin L Ebert, Michael A Gillette, Amanda Paulovich, Scott L Pomeroy, Todd R Golub, Eric S Lander, Jill P Mesirov, Gene set enrichment analysis: A knowledge-based approach for interpreting genome-wideexpression

profiles, Proc Natl Acad Sci U S A, 102 (2005 Oct 25) 15545-15550.
[32] Q. Wei, K. Mu, T. Li, Y. Zhang, Z. Yang, X. Jia, W. Zhao, W. Huai, P. Guo, L. Han, Deregulation of the NLRP3 inflammasome in hepatic parenchymal cells during liver cancer progression, Lab Invest, 94 (2014) 52-62.
[33] L. Hu, M. Chen, X. Chen, C. Zhao, Z. Fang, H. Wang, H. Dai, Chemotherapy-induced pyroptosis is mediated by BAK/BAX-caspase-3-GSDME pathway and inhibited by 2-bromopalmitate, Cell Death Dis, 11 (2020) 281.
[34] J. Yu, S. Li, J. Qi, Z. Chen, Y. Wu, J. Guo, K. Wang, X. Sun, J. Zheng, Cleavage of GSDME by caspase-3 determines lobaplatin-induced pyroptosis in colon cancer cells, Cell Death Dis, 10 (2019) 193.
[35] X. Zhang, P. Zhang, L. An, N. Sun, L. Peng, W. Tang, D. Ma, J. Chen, Miltirone induces cell death in hepatocellular carcinoma cell through GSDME-dependent pyroptosis, Acta Pharm Sin B, 10 (2020) 1397-1413.
[36] T. Hattori, Y. Takahashi, L. Chen, Z. Tang, C.A. Wills, X. Liang, H.G. Wang, Targeting the ESCRT-III component CHMP2A for noncanonical Caspase-8 activation on autophagosomal membranes, Cell Death Differ, 28 (2021) 657-670.
[37] E. De Schutter, L. Croes, J. Ibrahim, P. Pauwels, K. Op de Beeck, P. Vandenabeele, G. Van Camp, GSDME and its role in cancer: From behind the scenes to the front of the stage, Int J Cancer, 148 (2021) 2872-2883.
[38] M. Jiang, L. Qi, L. Li, Y. Li, The caspase-3/GSDME signal pathway as a switch between apoptosis and pyroptosis in cancer, Cell Death Discov, 6 (2020) 112.
[39] J. Lachner, V. Mlitz, E. Tschachler, L. Eckhart, Epidermal cornification is preceded by the expression of a keratinocyte-specific set of pyroptosis-related genes, Sci Rep, 7 (2017) 17446.
[40] T. Zhang, Y. Li, R. Zhu, P. Song, Y. Wei, T. Liang, G. Xu, Transcription Factor p53 Suppresses Tumor Growth by Prompting Pyroptosis in Non-Small-Cell Lung Cancer, Oxid Med Cell Longev, 2019 (2019) 8746895.
[41] Ł. Liszka, Pan-p63 but not ΔNp63 (p40) expression in undifferentiated carcinoma of the pancreas, Pol J Pathol, 71 (2020) 155-172.
[42] Y. Ma, Y. Chen, C. Lin, G. Hu, Biological functions and clinical significance of the newly identified long noncoding RNA RP185F18.6 in colorectal cancer, Oncol Rep, 40 (2018) 2648-2658.
[43] H. Zhu, A. Santo, Z. Jia, Y. Robert Li, GPx4 in Bacterial Infection and Polymicrobial Sepsis: Involvement of Ferroptosis and Pyroptosis, React Oxyg Species (Apex), 7 (2019) 154-160.
[44] B. Chao, F. Jiang, H. Bai, P. Meng, L. Wang, F. Wang, Predicting the prognosis of glioma by pyroptosis-related signature, J Cell Mol Med, 26 (2022) 133-143.
[45] Z.H. Wu, Z.W. Li, D.L. Yang, J. Liu, Development and Validation of a Pyroptosis-Related Long Non-coding RNA Signature for Hepatocellular Carcinoma, Front Cell Dev Biol, 9 (2021) 713925.

**Figure legend**

**Fig. 1 Workflow diagram. The specific workflow graph of data analysis.**

**Fig. 2 Differentially Expressed PRGs in the TCGA Cohort and Landscape of genetic and expression variation of PRGs in HCC.**

(A) The expression of 52 PRGs in normal tissues and HCC tissues.

(B) The mutation frequency and classification of 52 PRGs in HCC.

(C) The location of CNV alteration of 52 PRGs on 23 chromosomes in the HCC cohort.
(D) The CNV variation frequency of 52 PRGs in the HCC cohort. The height of the column represented the alteration frequency.
***P < 0.001, **P < 0.01, *P < 0.05.

**Fig. 3 Tumour classification based on the pyroptosis-related DEGs.**
(A) 374 HCC patients were divided into two clusters according to the consensus clustering matrix (k=2).
(B) Heatmap and the clinicopathologic characters of the two clusters classified by these DEGs.
(C) Kaplan–Meier OS curves for the two clusters.

**Fig. 4 Construction of risk signature in the TCGA cohort.**
(A) Univariate Cox regression analysis was used for screening of the survival-related pyroptosis genes.
(B) Distribution of patients based on the risk score in the TCGA cohort.
(C) The survival status for each patient in the TCGA cohort (low-risk population: on the left side of the dotted line; high-risk population: on the right side of the dotted line).
(D) Kaplan–Meier curves for the OS of patients in the low-risk group and high-risk group in the TCGA cohort.
(E) ROC curves demonstrated the predictive efficiency of the risk score in the TCGA cohort.

**Fig. 5 Validation of the risk model in the GEO cohort.**
(A) Distribution of patients in the GEO cohort based on the median risk score in the TCGA cohort.
(B) The survival status for each patient in the GEO cohort (low-risk population: on the left side of the dotted line; high-risk population: on the right side of the dotted line).
(C) Kaplan–Meier curves for the OS of patients in the low-risk group and high-risk group in the GEO cohort.
(D) ROC curves demonstrated the predictive efficiency of the risk score in the GEO cohort.

**Fig. 6 Univariate and multivariate Cox regression analyses for the risk score.**
(A) Univariate analysis of risk score and clinicopathological characteristics.
(B) Multivariate analysis of risk score and clinicopathological characteristics.
(C) Heatmap for the connections between clinicopathologic features and the risk groups (*P < 0.05).

**Fig. 7 Establishment and evaluation of a nomogram based on the TCGA dataset.**
(A) A nomogram for predicting 1-year, 3-year and 5-year OS.
(B) The calibration curves for predicting 1-year, 3-year and 5-year OS.
(C) The areas under the ROC curves for predicting 1-year, 3-year and 5-year OS.

**Fig. 8 The relationship between prognostic signature and immune response.**
(A) A detailed Spearman correlation analysis was performed using different algorithms.
(B) The heatmap of immune responses based on different algorithms among the high- and low-risk group.

**Fig. 9 Gene set enrichment analysis (GSEA) and lower half inhibitory centration (IC50) of chemotherapeutic drugs between the high- and low-risk group based on the pyroptosis-related genes signature in TCGA-HCC.**

(A) GSEA results suggested that the two risk groups were mainly enriched in tumor immunity and metabolism.

(B) A low-risk score was related to IC50 of chemotherapeutics such as Gemcitabine, Nilotinib, Camptothecin, Tipifarnib and a high-risk score was related to Axitinib, Dasatinib, Erlotinib, Lapatinib.

**Fig. 10 Functional analysis based on the DEGs between the two-risk groups in the TCGA cohort.**

(A) Bubble graph for GO enrichment (the bigger bubble means the more genes enriched, and the increasing depth of red means the differences were more obvious).

(B) Barplot graph for KEGG pathways (the longer bar means the more genes enriched, and the increasing depth of red means the differences were more obvious).

**Fig. 11 Validated PRGs between HCC Tissues and Adjacent Normal Tissues.**

(A-J) BAK1, BAX, CHMP2A, GSDME, IL1A, TP53, TP63, GPX4, PRKACA and SCAF11 in HCC tissues.

**Supplementary Fig. S1 Expressions of the 42 PRGs and the interactions among them.**

(A) PPI network showing the interactions of the PRGs (interaction score = 0.9).

(B) The correlation network of the PRGs (red line: positive correlation; blue line: negative correlation. The depth of the colours reflects the strength of the relevance).

**Supplementary Fig. S2 The correlation of gene expression with each type of immune cell infiltration.**

(A) The correlation of gene expression with each type of immune cell infiltration.

**Supplementary Fig. S3 The result of alteration frequency between the high- and low-risk group.**

(A) The top 20 driver genes with the highest alteration in the high-risk group.

(B) The top 20 driver genes with the highest alteration in the low-risk group.

# Figures

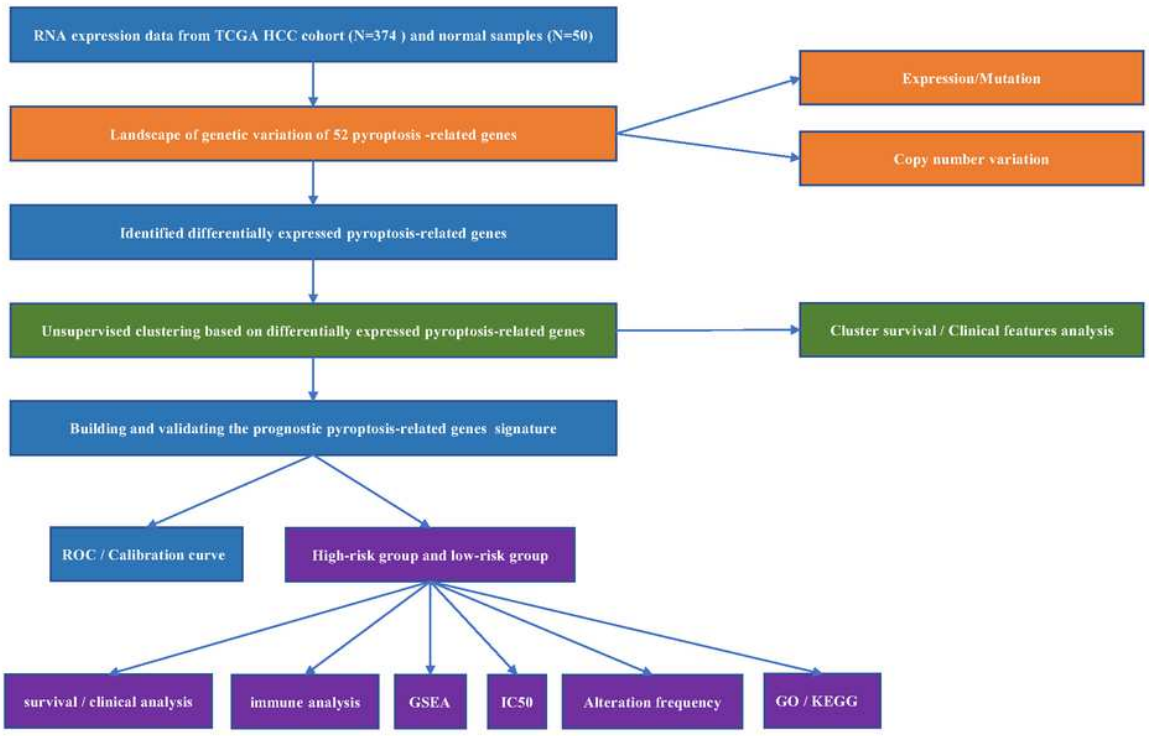


**Figure 1**

Workflow diagram. The specific workflow graph of data analysis.

**Figure 2**

Differentially Expressed PRGs in the TCGA Cohort and Landscape of genetic and expression variation of PRGs in HCC. (A) The expression of 52 PRGs in normal tissues and HCC tissues. (B) The mutation frequency and classification of 52 PRGs in HCC. (C) The location of CNV alteration of 52 PRGs on 23 chromosomes in the HCC cohort. (D) The CNV variation frequency of 52 PRGs in the HCC cohort. The height of the column represented the alteration frequency. ***P < 0.001, **P < 0.01, *P < 0.05.

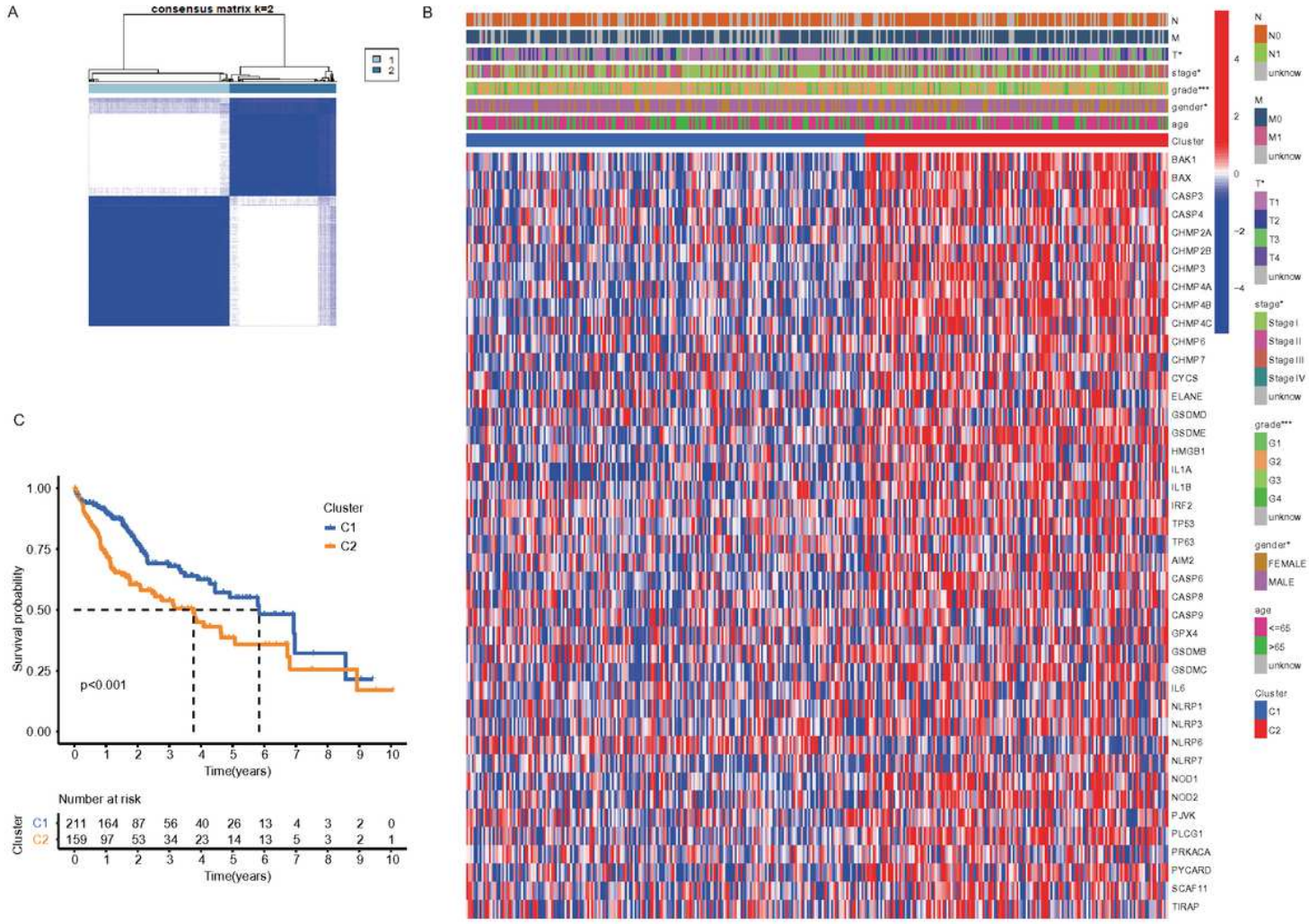


## Figure 3

Tumour classification based on the pyroptosis-related DEGs. (A) 374 HCC patients were divided into two clusters according to the consensus clustering matrix (k=2). (B) Heatmap and the clinicopathologic characters of the two clusters classified by these DEGs. (C) Kaplan–Meier OS curves for the two clusters.

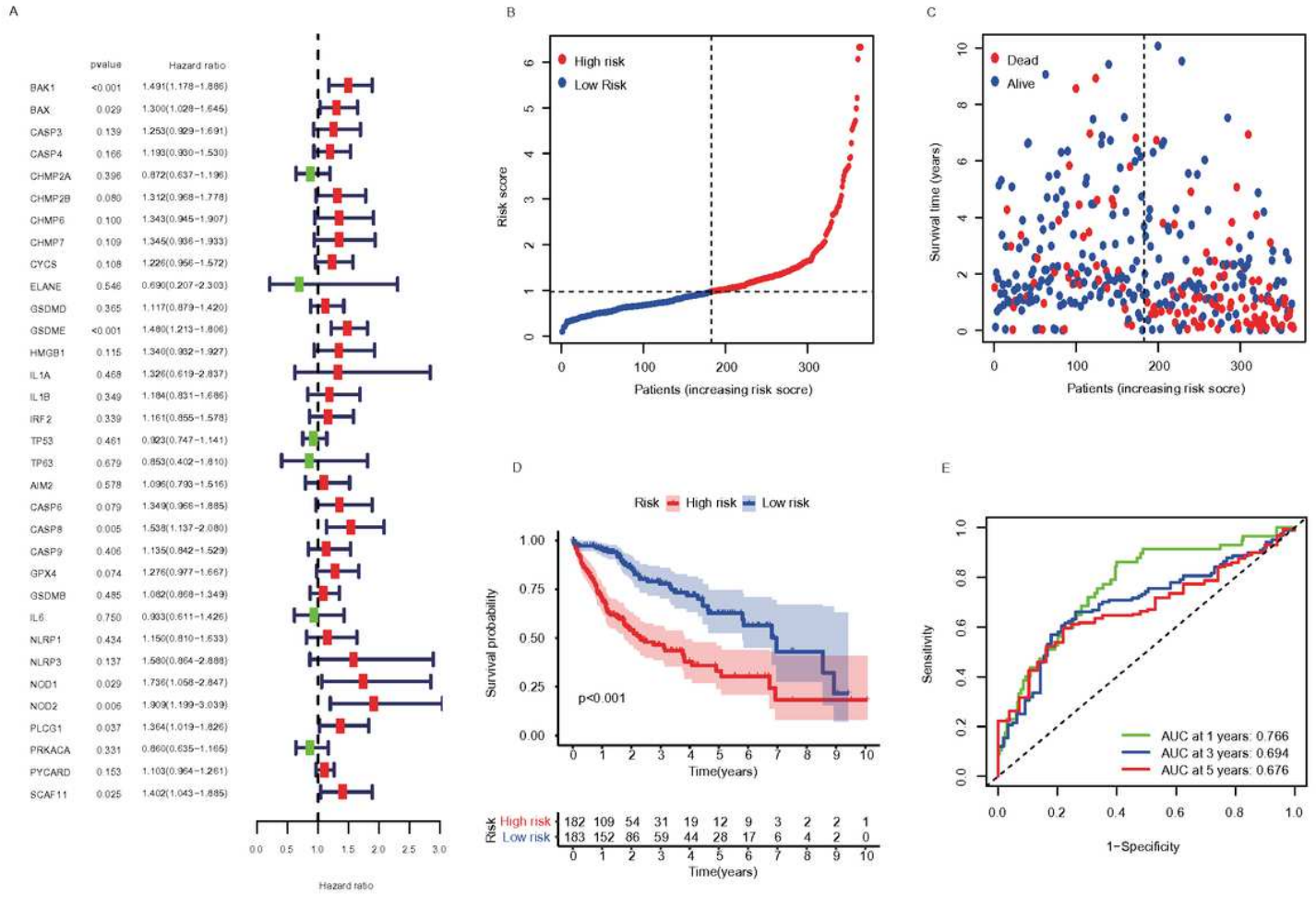


## Figure 4

Construction of risk signature in the TCGA cohort. (A) Univariate Cox regression analysis was used for screening of the survival-related pyroptosis genes. (B) Distribution of patients based on the risk score in the TCGA cohort. (C) The survival status for each patient in the TCGA cohort (low-risk population: on the left side of the dotted line; high-risk population: on the right side of the dotted line). (D) Kaplan–Meier curves for the OS of patients in the low-risk group and high-risk group in the TCGA cohort. (E) ROC curves demonstrated the predictive efficiency of the risk score in the TCGA cohort.

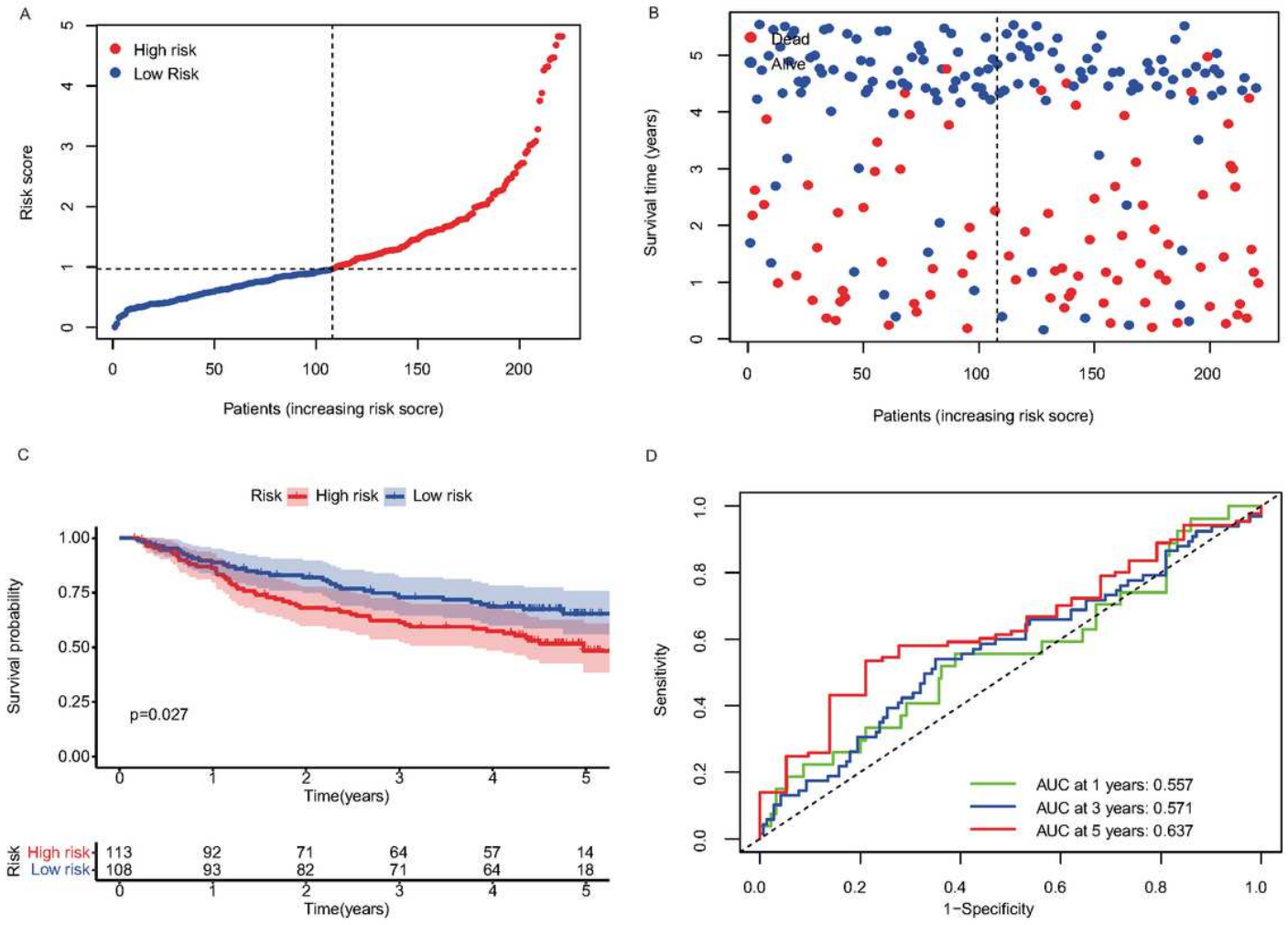


## Figure 5

Validation of the risk model in the GEO cohort. (A) Distribution of patients in the GEO cohort based on the median risk score in the TCGA cohort. (B) The survival status for each patient in the GEO cohort (low-risk population: on the left side of the dotted line; high-risk population: on the right side of the dotted line). (C) Kaplan–Meier curves for the OS of patients in the low-risk group and high-risk group in the GEO cohort. (D) ROC curves demonstrated the predictive efficiency of the risk score in the GEO cohort.

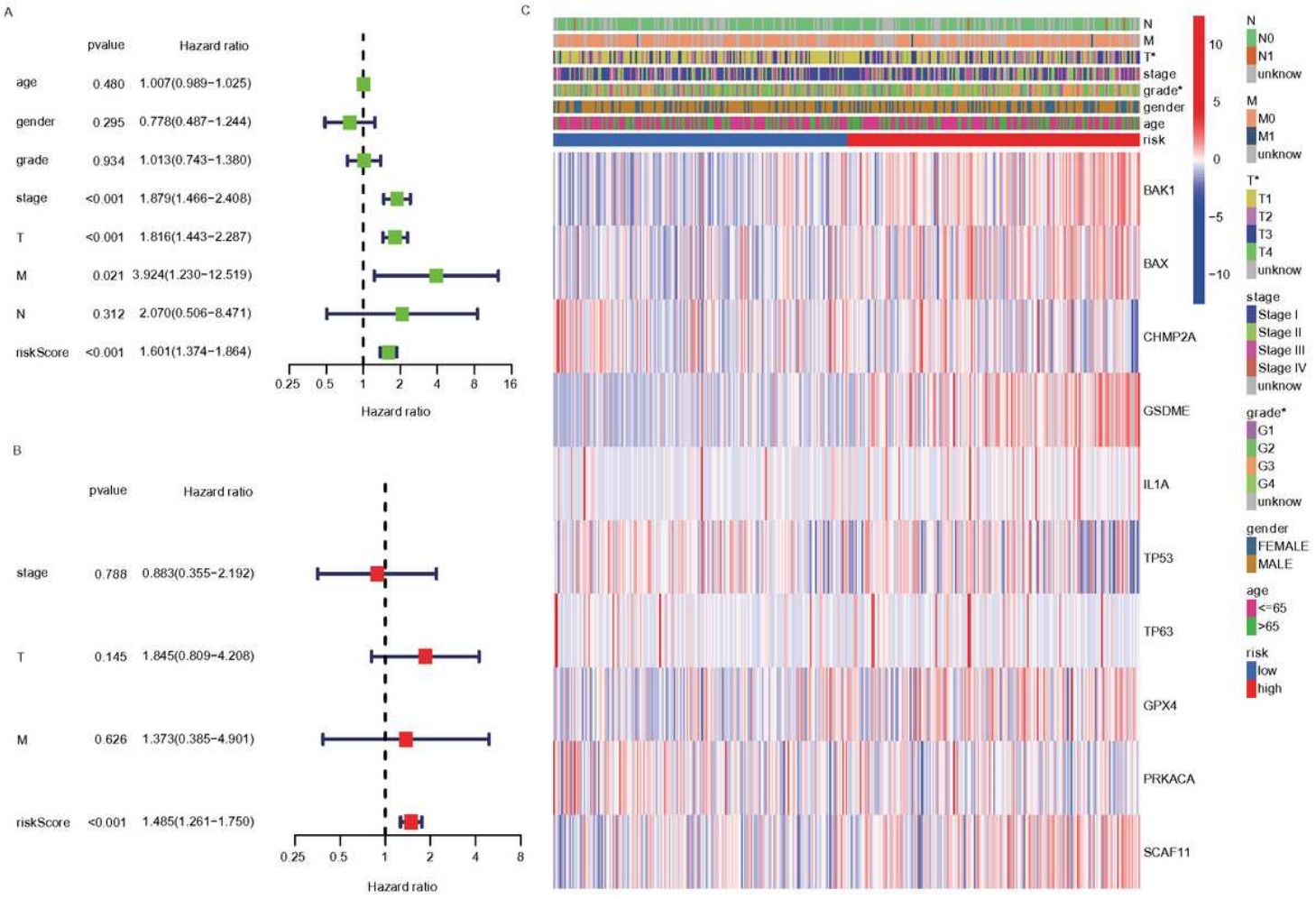


## Figure 6

Univariate and multivariate Cox regression analyses for the risk score. (A) Univariate analysis of risk score and clinicopathological characteristics. (B) Multivariate analysis of risk score and clinicopathological characteristics. (C) Heatmap for the connections between clinicopathologic features and the risk groups (*P < 0.05).

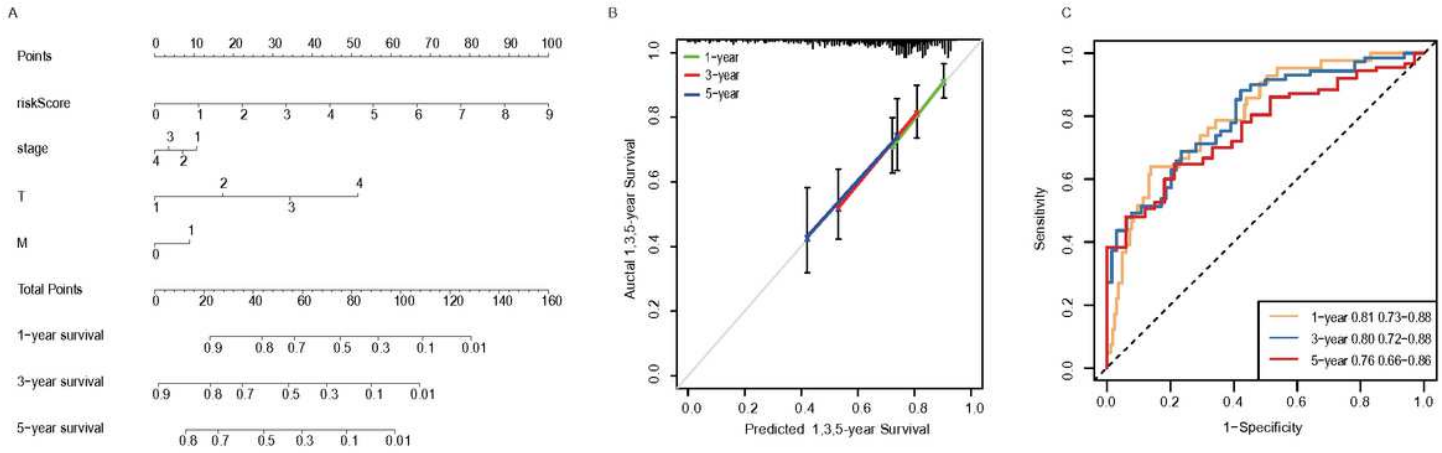


## Figure 7

Establishment and evaluation of a nomogram based on the TCGA dataset. (A) A nomogram for predicting 1-year, 3-year and 5-year OS. (B) The calibration curves for predicting 1-year, 3-year and 5-year OS. (C) The areas under the ROC curves for predicting 1-year, 3-year and 5-year OS.

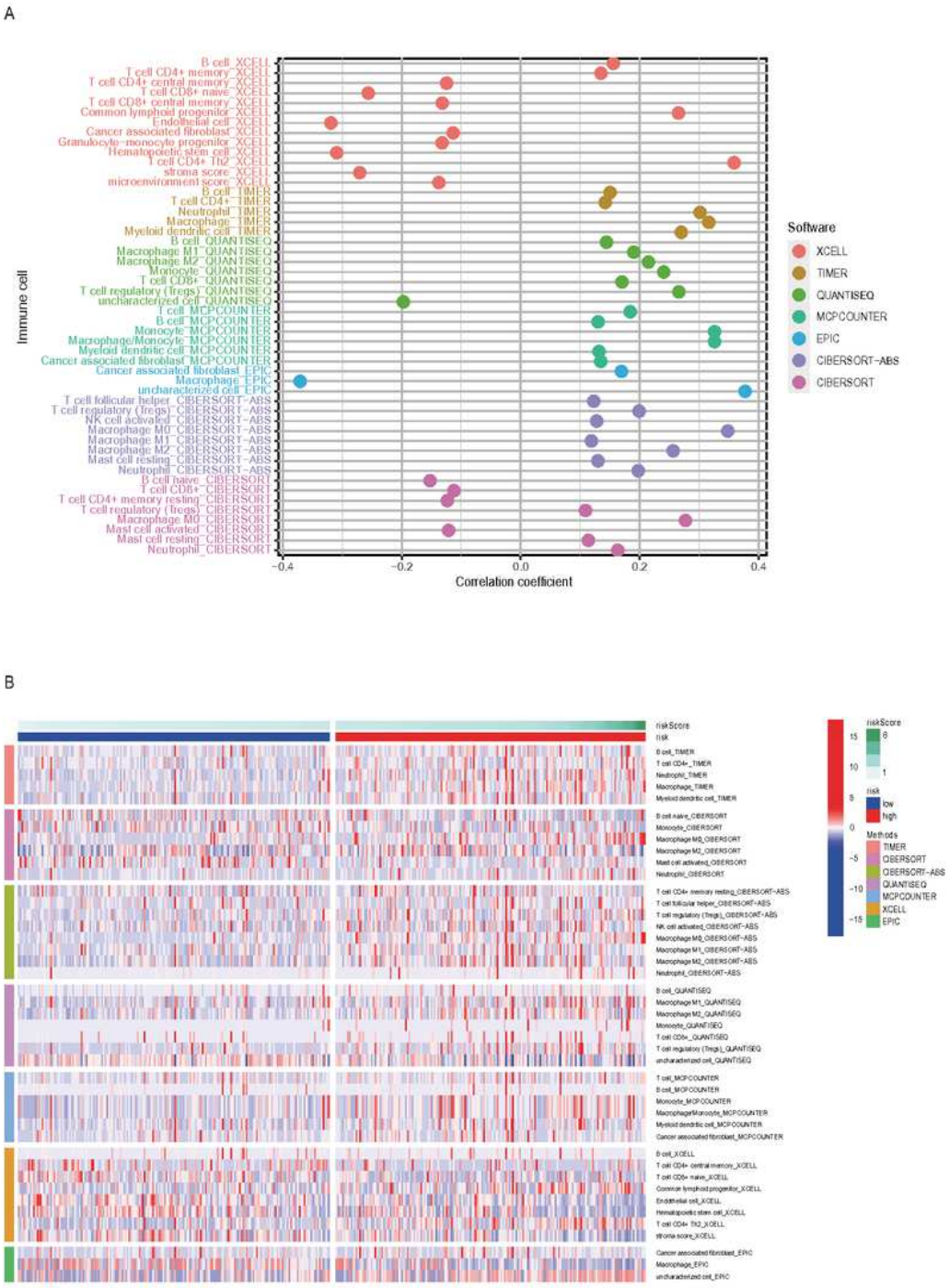


## Figure 8

The relationship between prognostic signature and immune response. (A) A detailed Spearman correlation analysis was performed using different algorithms. (B) The heatmap of immune responses based on different algorithms among the high- and low-risk group.

**Figure 9**

Gene set enrichment analysis (GSEA) and lower half inhibitory centration (IC50) of chemotherapeutic drugs between the high- and low-risk group based on the pyroptosis-related genes signature in TCGA-HCC. (A) GSEA results suggested that the two risk groups were mainly enriched in tumor immunity and metabolism. (B) A low-risk score was related to IC50 of chemotherapeutics such as Gemcitabine, Nilotinib, Camptothecin, Tipifarnib and a high-risk score was related to Axitinib, Dasatinib, Erlotinib, Lapatinib.

**Figure 10**

Functional analysis based on the DEGs between the two-risk groups in the TCGA cohort. (A) Bubble graph for GO enrichment (the bigger bubble means the more genes enriched, and the increasing depth of red means the differences were more obvious). (B) Barplot graph for KEGG pathways (the longer bar means the more genes enriched, and the increasing depth of red means the differences were more obvious).

**Figure 11**

Validated PRGs between HCC Tissues and Adjacent Normal Tissues. (A-J) BAK1, BAX, CHMP2A, GSDME, IL1A, TP53, TP63, GPX4, PRKACA and SCAF11 in HCC tissues.

## Supplementary Files

This is a list of supplementary files associated with this preprint. Click to download.

- TableS1.xlsx
- TableS2.xlsx
- Fig.S1.jpg
- Fig.S2.pdf
- Fig.S3.pdf